Tian ZHOU[1], Haisen LI[1], Jian XU[1], Chao XU[1]

Science and Technology on Underwater Acoustic Laboratory, Harbin Engineering University, Harbin, People's Republic of China (1)

Research on the dot-by-dot imaging algorithm for multi-beam SAS with multi-frequency in azimuth

Abstract. *In multi-beam synthetic aperture sonar (SAS), the smaller the transmit sensor array's physics aperture is, the larger its synthetic aperture length is, and then the better its along-track resolution will be. But when the physics aperture is small, the mapping speed should be limited to avoid the azimuth ambiguity. In order to overcome this problem, a scheme of multi-beam SAS with multi-frequency in azimuth is proposed in this paper based on the sensor array configuration and basic principle of multi-beam SAS. A correlated math model is presented and the dot-by-dot imaging algorithm is simulated according to the new scheme. Compared with the primary multi-beam SAS scheme proposed before, the new scheme can improve the along-track resolution and increase the mapping speed. Computer simulation results are given to test the correctness and efficiency of the new scheme.*

Streszczenie. *W artykule przedstawiono nową strukturę wielowiązkowego sensora SAS, pozwalającą na eliminację problemów związanych z dwuznacznością azymutu. Proponowane rozwiązanie bazuje na podstawowych zasadach działania SAS oraz odpowiedniej konfiguracji tablicy czujników. Zbudowano także model matematyczny oraz opracowano algorytm pozwalający na obrazowanie działania punkt po punkcie. Dokonano weryfikacji symulacyjnej proponowanej struktury. (**Badania wielowiązkowego sensora SAS – zagadnienie dwuznaczności azymutu i algorytm obrazowania punkt po punkcie**).*

Keywords: underwater acoustic sensor array, synthetic aperture sonar, multi-beam, multi-frequency, dot-by-dot imaging.
Słowa kluczowe: tablica podwodnych czujników dźwięku, sensor SAS, wielowiązkowy, wieloczęstotliwościowy, obrazowanie dot-by-dot.

1. Introduction

Multi-beam bathymetry sonar is one of the important equipments for bathymetry surveying, ocean exploitation and seabed imaging. It forms several beams in the vertical plane of the ship's track using the beamforming technique and it can obtain the depth information of each beam by signal processing. Compared with side-scan sonar, multi-beam sonar has the advantages of wide coverage and high efficiency [1, 2, 3]. However, because multi-beam bathymetry sonar array is generally installed on the surveying ship far away from the seafloor, the footprints formed in the seafloor are large, which makes its along-track resolution lower than side side-scan sonar.

Although the physical aperture is small, synthetic aperture technique can synthesize the effect of a large aperture taking advantage of the phase history from ping to ping, and obtain high along-track resolution [4, 5]. The array architecture of conventional synthetic aperture sonar (SAS) is based on side-scan sonar, it can only get the slant range and azimuth information of the target, cannot get the depth and distance information of the target [6, 7, 8, 9].

Taking account of the problems above, Yao proposes a new scheme of a primary multi-beam synthetic aperture sonar basing on the combination of the multi-beam bathymetry and aperture synthetic principle [10, 13], which synthesizes the outputs of the receiving beams from the same direction in each ping in cross-track direction based on the Mill's crossing array generally used in multi-beam bathymetric sonar, and consequently improves the along-track resolution. In order to improve the mapping speed of the primary multi-beam synthetic aperture sonar proposed in the article [10], here we further present a new scheme of multi-beam SAS with multi-frequency in azimuth and simulate the dot-by-dot imaging algorithm according to the scheme. The results show that, the new scheme not only has all the advantages of the primary multi-beam SAS, but also can overcome the contradiction between the mapping speed and azimuth ambiguity well.

2. Principle and math model of the new multi-beam SAS

2.1. Principle of multi-frequency in azimuth

Fig.1(a) shows the signal transmission geometry of transmitting a single frequency beam in azimuth and Fig. 1(b) gives the signal transmission geometry of multi-beam SAS with multi-frequency in azimuth. The new multi-beam SAS uses the phased linear array as the transmitting array, which transmits several beams with different frequency along the track successively at each pulse transmitting time. We can see from Fig.1 (b) that in the mode of transmitting three adjacent beams, the effective synthetic aperture is about three times larger than the single transmitting beam mode, which means that the azimuth resolution of the new multi-beam SAS maybe is three times higher than the primary multi-beam SAS. The following parts will analyze in detail why multi-beam with multi-frequency can improve the azimuth resolution and the mapping speed.

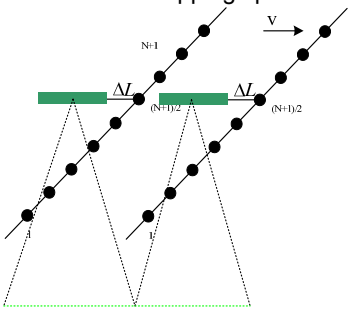

(a) Transmitting a single frequency beam (primary).

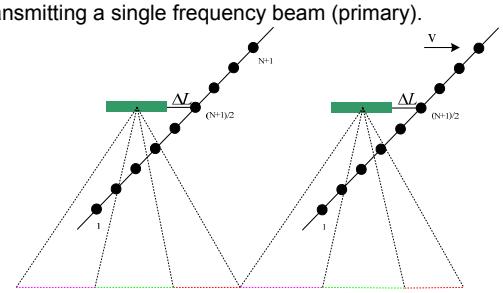

(b) Transmitting several adjacent beams with different frequencies (new).

Fig.1.Two different signal transmission geometries of multi-beam SAS.

Assumed that the total length along the track of the transmitting array is *3D*, and we use three adjacent transmitting beams whose wavelength respectively is λ_L, λ_M and λ_R to synthetic aperture, then the total width of the horizontal beam along the track can be expressed as follows

(1) $$\theta = \frac{\lambda_M}{3D} + \frac{\lambda_L}{3D}\partial_L + \frac{\lambda_R}{3D}\partial_R$$

Where, ∂_L and ∂_R are the directional factors of the left and right beams respectively.

The effective length of synthetic aperture at the distance R is

(2) $$L_{eff} = R\theta = \frac{R}{3D}(\lambda_M + \lambda_L\partial_L + \lambda_R\partial_R)$$

Now the azimuth resolution can be described as

(3)
$$\Delta X_s = \theta_s R \le \frac{\max(\lambda_M, \lambda_L, \lambda_R)}{2L_{eff}} R = \frac{\max(\lambda_M, \lambda_L, \lambda_R)}{\lambda_M + \lambda_L\partial_L + \lambda_R\partial_R} \cdot \frac{3D}{2}$$

When the frequency differences of the selected three signal pulses are small, their wavelength differences will be small too, and ∂_L and ∂_R are approximately equal to 1. Then we can simplify the equation (3) as

(4) $$\Delta X_s \approx \frac{1}{3} \cdot \frac{3D}{2} = \frac{D}{2}$$

We can see from the above equation that the azimuth resolution in the multi-beam SAS with multi-frequency in azimuth has been improved than that of the primary multi-beam SAS transmitting a single frequency beam.

In addition, when using only one transmitting array which length is D, in order to reach the azimuth resolution "D/2" and avoid azimuth ambiguity, the sampling interval must be smaller or equal to D/2. However, the new multi-beam SAS with a transmitting array whose length is 3D can reach the D/2 azimuth resolution while the sampling interval is smaller or equal to 3D/2. Obviously, the new scheme can improve the mapping speed of multi-beam of SAS without sacrificing of resolution.

2.2. Math model

Fig.2 shows the echo receiving geometry of multi-beam SAS with multi-frequency, where the sonar array has a"T"shaped structure, including a multi-element transmitting array and a multi-element receiving array.

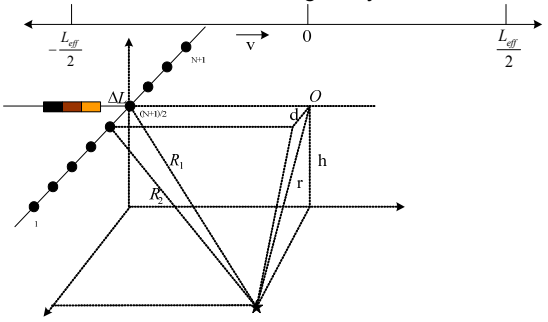

Fig.2. The echo receiving geometry of multi-beam SAS

The distance between the transmitting array and receiving array is ΔL ,the effective synthetic aperture length is L_{eff}. Assumed that the moving speed of sonar array is v, and transmitting array transmits three adjacent pulse beams at each pulse transmitting time. The three pulses are LFM signals with different frequency

(5) $$s_m(t) = p_0(t)\exp(j\omega_m t)$$

(6) $$p_0(t) = rect(t/T)\exp(j\pi\mu t^2)$$

Where, m is the number index of different pulse beam (m = 1, 2, 3), $p_0(t)$ is the envelope of the signal, T is the chirp length, ω_m is carrier frequency, μ is the chirp rate. When the transmitting array location coordinate is X_T, the range between the transmitting array and target located at $(0, r)$ is

(7) $$R_{tra}(X_T, r) = \sqrt{X_t^2 + r^2}$$

Where, r is the slant range of the target. The path length between N+1 receiving element and target can be expressed as

(8) $$R_{rec}(n, X_t) = \sqrt{\begin{matrix}(X_t + \frac{D}{2} + \Delta L)^2 + ((\frac{N+1}{2} - n)d)^2 \\ +r^2 - 2(\frac{N+1}{2} - n)d\sqrt{r^2 - h^2}\end{matrix}}$$

Where, n is the number index of receiving array element (n=1,2,…,N+1)， d is the sampling space along the track, h is the depth of target.

3. The dot-by-dot imaging algorithm for the new scheme

3.1. The multi-beam receiving model in cross-track direction

The multi-beam SAS with multi-frequency uses a receiving array in cross-track direction vertical to the transmitting array to receive the echoes, and controls the beam angle to different direction with beamforming technique. We take a single point target as an example, because at each sampling position the three multi-frequency beams have a certain interval, the three echoes from different beams have a delay in slant-range direction between each other. Assumed that the interval between the adjacent beams at the same sampling location is Δt, and the target can only be observed by the *mth* beam when the transmitting array is at the location X_T, the echo received by the *nth* element of receiving array can be expressed as

(9) $$e_n(t) = s_m\left(t - \frac{R_{rec}(n, X_T) + R_{tra}(X_T, r)}{c} - (m-1)\Delta t\right)$$

Where, m is the number index of pulse beams with different frequencies (m = 1, 2, 3).

We can see from equation (9) that, the echo received by the receiving elements comes from different transmitting beam at different sampling location. In order to apply beamforming algorithm to the echo data, we need to compensate the time delay Δt to the echo which comes from the second transmitting beam and $2\Delta t$ to the third transmitting beam. Then we can process the echo of the cross-track receiving array by conventional beamforming algorithm, and get the outputs of beams with different angles. The output of the beam the point target existing in is

(10) $$y(t) = \sum_{n=1}^{n=N+1} e_{\frac{N+1}{2}}(t)$$

Where, n is the number index of receiving array element (n=1,2,…,N+1).

3.2. The dot-by-dot imaging algorithm

Dot-by-dot imaging algorithm is also called as time-domain interfering accumulation algorithm. Its principle is, to calculating the time delay of each receiving location in the range of the virtual synthetic aperture first, then to compensating the time delay to implement the focused beamforming, and finally getting the image [11-12]. In order to achieve the high range resolution, we should correlate the received echo with the transmitted pulse to make the echo compressed into a narrow pulse before dot-by-dot imaging. The concept of the dot-by-dot algorithm is clear, simple, and its imaging result is accurate. That's why we choose this algorithm in this paper to express the superiority of the new scheme.

Conventional SAS dot-by-dot imaging algorithm can be applied to these outputs of beams with the same steering

angle in different pings, and then the imaging result of target can be got. The depth H and cross-track distance Y can be obtained by the equation

$$\begin{cases} H = r_0 \cos(\theta_0) \\ Y = r_0 \sin(\theta_0) \end{cases} \tag{11}$$

At last, the total image of the transmitted fan-shaped beam can be got by synthesizing the image of different receiving beams.

4 Computer simulation and performance analysis

In order to verify the advantages of the multi-beam SAS system and the algorithm proposed in this paper, simulation and detailed comparison among the conventional multi-beam bathymetry sonar, traditional SAS, primary multi-beam SAS and the improved scheme of multi-beam SAS are done in this section.

4.1. Compared with the conventional multi-beam sonar

The simulation scene is a single point target, the parameters are as follows. The single point target P_1 slant range r_1=52m , azimuth coordinate x_1=0m, depth h_1=45.0333m (the angle between the slant range r_1 and the depth h_1 is $\pi/6$, and its cross-track distance is 26m), the transmitting array length 0.6m, the bandwidth B=2kHz, chirp length T=5ms, the number of receiving elements is 32, the number of cross-track beam is 51, v=3m/s, pulse repetition frequency f_r=10Hz, sound speed c=1500m/s, the sampling frequency f_s=150kHz. Using the single pulse model with the carrier frequency f_m=20kHz, the imaging result of the conventional multi-beam sonar is as Fig. 3(a), while using the multi-frequency and multi-beam SAS with three adjacent pulses whose carrier frequency respectively is f_l=27.5kHz, f_m =20kHz, f_r =35kHz, the imaging result got with the new multi-beam SAS is showed in Fig.3 (b).

Fig. 3(a) stands for the imaging result of the P_1 with the conventional multi-beam sonar. Because the conventional multi-beam sonar cannot distinguish the different targets in the same along-track beam, its imaging result is almost a light line. We can see that the imaging result with the new multi-beam SAS is a light point in Fig. 3(b). Obviously, the scheme proposed in this paper can improve the along-track resolution of multi-beam bathymetry sonar effectively.

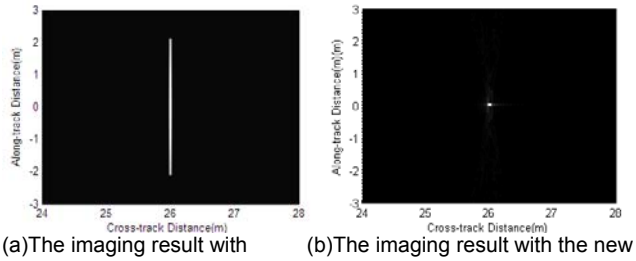

(a)The imaging result with multi-beam sonar (b)The imaging result with the new multi-beam SAS

Fig.3. Compared with the conventional multi-beam sonar

4.2. Compared with the traditional SAS

Parameters are the same as section 4.1. The coordinate of another point target P_2 is (x, r, θ) = (0, 52, π/3), where x is the location along the track, r is the slant range, the target is in the direction of beam whose steering angle is θ. The target P_1 and P_2 are in the plane with the same along-track location, but they are in the different receiving beams. In other words, their depths and distances are different. The imaging results with traditional SAS and multi-beam SAS are shown in Fig. 4.

Fig. 4 (a) is the imaging result of P_1 and P_2 estimated with traditional SAS, which can only illustrate the target from slant range and azimuth. Their image is just one bright point whose slant range is 52m. Fig. 4 (b) shows the result estimated with the multi-beam SAS, which can give the cross-track distance and depth information of targets because multi-beam SAS can image targets in different beams. The three-dimension location of targets is shown in Fig. 4 (c), from which we can see that the depths of two targets are respectively 45.003m and 26 m, their cross-track distances are respectively 26m and 45.003m.

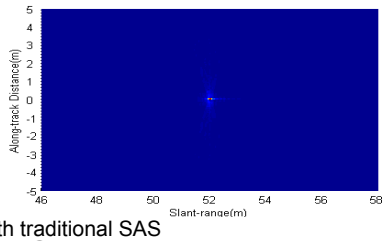

(a) Result with traditional SAS

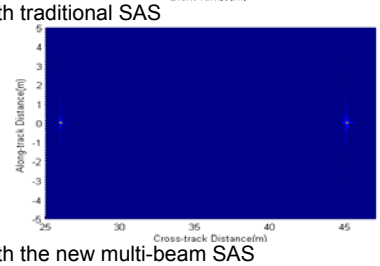

(b) Result with the new multi-beam SAS

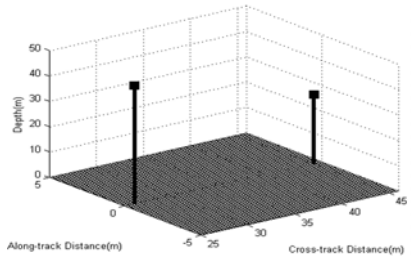

(c) Three-dimension location of targets

Fig.4. Results of target P1 and P2 got by traditional SAS and the new multi-beam SAS

4.3. Compared with the primary multi-beam SAS

(1)The comparison of along-track resolution

The coordinate of a point target P_3 is (x, r, θ) = (0.2, 52,π/6), whose depth is 45.0333m, the cross-track distance is 26m and the other parameters are the same as section 4.1. The imaging results of P_1 and P_3 got respectively from primary multi-beam SAS and the new multi-beam SAS with multi-frequency in azimuth are shown in Fig. 5 and Fig.6.

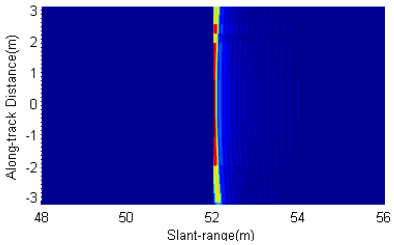

(a) Compressed echo

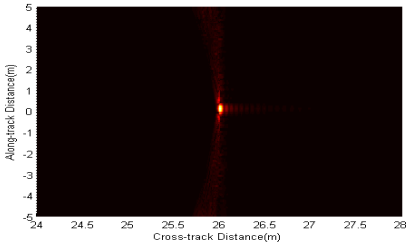

(b) Focused image

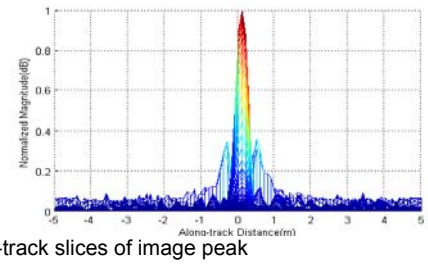

(c) Along-track slices of image peak

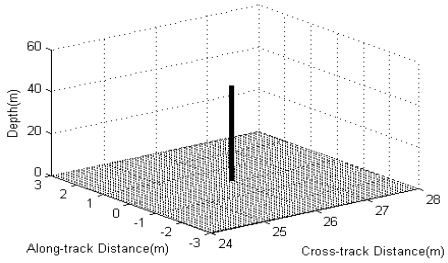

(d) Depth results

Fig.5. Results of P1 and P3 with the primary multi-beam SAS

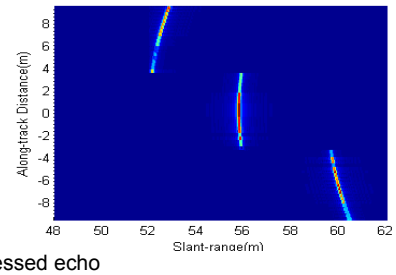

(a) Compressed echo

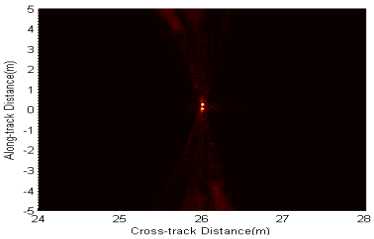

(b) Focused image

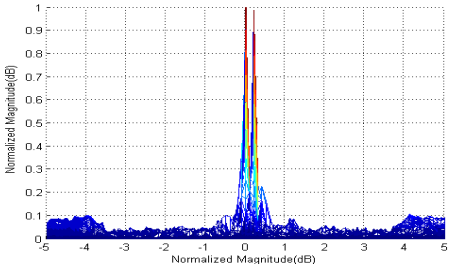

(c) Along-track slices of image peak

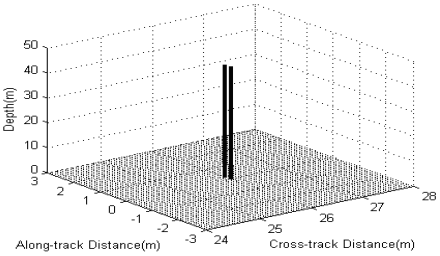

(d) Depth results

Fig.6. results of P1 and P3 with the new multi-beam SAS

Fig.5(a) and Fig.6(a) respectively show the compressed echo of the primary multi-beam SAS and the multi-beam SAS with multi-frequency in azimuth. We can see that the effective synthetic aperture showed in Fig. 6(a) is about three times larger than the one showed in Fig. 5(a). Because the new scheme transmits three adjacent beams successively, the echo showed in Fig. 6(a) is divided into three parts, which have a pulse length delay between each other. Fig. 5(b) and Fig. 6(b) are the focused image got by the two different schemes, Fig. 5(c) and Fig. 6(c) are the along-track slices of image peak and Fig. 5(d) and Fig. 6(d) are the depth results estimated.

We can see from Fig. 5(b) and (c) that, primary multi-beam SAS cannot distinguish the targets 0.2m apart in along-track direction because its along-track resolution can only reach 0.3m theoretically. But multi-beam SAS with multi-frequency in azimuth can distinguish the two targets because its along-track resolution can reach 0.1m, Fig. 6(b) and (c) have showed the better imaging results. Therefore, the new scheme proposed in this paper has a more excellent along-track resolution than primary multi-beam SAS.

(2)The comparison of mapping speed

The simulation scene is the single point target P1 described in section 4.1, the bandwidth B=2kHz, chirp length T=5ms, the number of receiving elements is 32, the number of cross-track beam is 51, v=3m/s, pulse repetition frequency fr=10Hz, sound speed c=1500m/s, the sampling frequency fs=150kHz. In the imaging scheme of the primary multi-beam SAS, the length of transmitting array is 0.2m, the carrier frequency fm=30kHz, and the imaging result is showed as Fig. 7. In the new scheme of multi-beam SAS with three adjacent pulses in azimuth, whose carrier frequency respectively is fl=22.5kHz, fm=30kHz, fr=37.5kHz, the transmitting array length is 0.6m, and the imaging result is showed as Fig. 8.

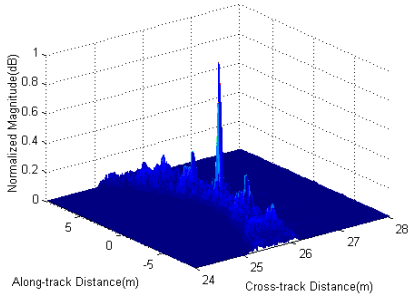

(a)Focused image

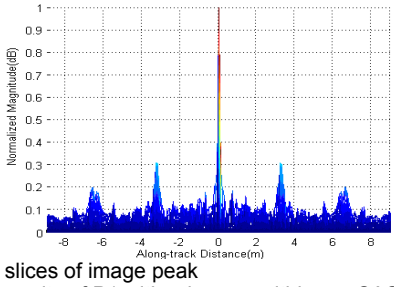

(b) Along-track slices of image peak

Fig.7. Imaging results of P1 with primary multi-beam SAS (the length of transmitting array is 0.2m)

We can see from Fig. 7(a) and (b) that, there are aliased targets in the imaging result got by the primary multi-beam SAS when the length of transmitting array is 0.2m. The reason for this is that the sampling interval in azimuth D_{pulse1} (D_{pulse1}= v/f_r =0.3m) is greater than half of the transmitting array's length. In order to avoid the aliased targets, we should make the sonar move slower to make the sampling interval less than or equal to half of the transmitting array's length.

The sampling interval of the new multi-beam SAS is 0.3m, and its transmitting array's length is 0.6m which is equal to half of the transmitting array's length. Then there are not aliased targets in the imaging result got by the new

multi-beam SAS as Fig.8 (a) and (b) showed. The lengths of effective synthetic aperture in Fig. 7 and Fig.8 are same, so their azimuth resolution is same.

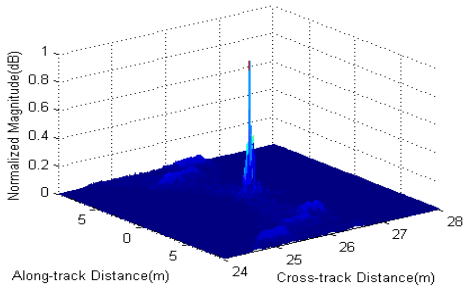

(a)Focused image

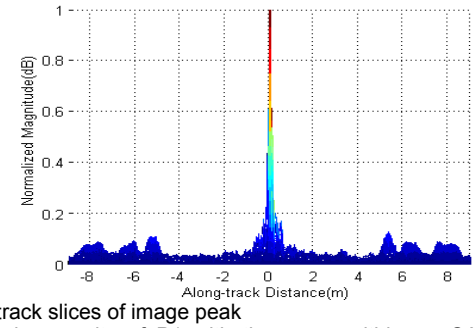

(b) Along-track slices of image peak

Fig.8. Imaging results of P1 with the new multi-beam SAS (the length of transmitting array is 0.6m)

From the above comparison and analysis, the following conclusion can be drawn: when the demand for azimuth resolution is same, the multi-beam SAS with multi-frequency in azimuth can have a larger mapping speed than the primary multi-beam SAS.

5 Conclusions

This paper proposes a scheme for the realization of the multi-beam SAS with multi-frequency in azimuth based on the multi-beam bathymetry and aperture synthetic principle. Its intent is to overcome the contradiction between the high mapping speed and azimuth resolution, and to enhance the along-track resolution of the primary multi-beam bathymetric sonar. The paper has introduced the basic principle of the new multi-beam SAS, established correlative math model and simulated the dot-by-dot imaging algorithm. Simulation results show that, the new multi-beam SAS not only has all the advantages of the primary multi-beam SAS, but also has the better azimuth resolution, which adequately proves the superiority, effectivity and feasibility of the scheme and the corresponding dot-by-dot imaging algorithm purposed in this paper.

Acknowledgment

Research in this paper was supported by National Natural Science Foundation of China (Grant No. 41076056 and 41006057), Research Fund for the Doctoral Program of Higher Education of China (Grant No. 20112304130003), and some Pre Research Foundation (Grant No.40102).

REFERENCES

[1] YAO Bin. Study on multiple sub-array special module underwater acoustic imaging technology.Harbin: Harbin Engineering University, 2009.

[2] MA Jian-lin, JIN Jin, LIU Qin. Multi-beam echosounder versus side scan object detection a comparative analysis. Hydrographic Surveying and Charting, 26(2006), No.3, 10-12.

[3] ZHOU Tian, LI Hai-sen, ZHU Zhi-de. Performance analysis of improved multiple sub-array detection method in multi-beam bathymetry system. Technical Acoustics,24(3005), No.3, 152-156.

[4] Michael P. Hayes, Peter T.Gough. Synthetic aperture sonar: a review of current status. IEEE Journal of Oceanic Engineering, 34(2009). No. 3, 207-224.

[5] Philippe Courmontagne, Thomas Telandro, Akira Asada. An improvement on SAS image formation. OCEANS '09 IEEE Bremen: Balancing Technology with Future Needs, Bremen, Germany, 2009, 1-8.

[6] Jiang X K, Sun C, Feng J.A novel image reconstruction for synthetic aperture sonar with single transmitter and multiple-receiver configuration. In: Proceedings of the IEEE Oceans 2004 Conference Proceedings, Kobe, Japan, 2004, 1940-1944.

[7] XU Jiang, TANG Jin-song, ZHANG Chun-hua. Beam formation imaging algorithm for synthetic aperture sonar. Signal Processing, 19 (2003), No. 2, 157-160.

[8] YANG Hai-liang, TANG Jin-song, ZHANG Sen. A chirp scaling imaging algorithm with non-uniform sampling in azimuth and without approximation of stop-and-hop for multiple-receiver synthetic aperture sonar. Chinese High Technology Letters, 19(2009), No. 9, 939-945.

[9] Hayden J Callow. Signal processing for synthetic aperture sonar image enhancement.New Zealand: University of Canterbury, Christchurch, 2003.

[10] Yao Yong-hong, Zhou Tian. Research on the dot-by-dot imaging algorithm for multi-beam SAS based on a new array configuration, Journal of electronics & information technology, accepted.

[11] Sawa T, Aoki T, Yoshida H. Modified synthetic aperture algorithm for sonar systems. International Journal of Adaptive Control and Signal Processing, 2010, 24(2010), No.2,142-148.

[12] LIU XIN-hua. Research on System Design and Image Reconstruction Algorithms for Interferometric Synthetic Aperture Sonar. Institute of Acoustics, Chinese Academy of Sciences. 2008, 19-22.

[13] Koun-Tem Sun, Hsin-Te Chan, Man-Ting Ku, Chang Fu-Yuan, Tzu-Wei Huang. An Application of Fourier Transformation and Back-propagation Neural Network for Brain-computer Interface Cursor Control, *Advanced Management Science,* 1(2011), No.1, 11-21.

***Authors**: Tian ZHOU, Haisen LI, Jian XU and Chao XU are with Room #806, Shuisheng building, the Science and Technology on Underwater Acoustic Laboratory of Harbin Engineering University, Harbin, China.*

(Email:zhoutian@hrbeu.edu.cn;hsenli@126.com;xujian@hrbeu.edu.cn; xuchao18@hrbeu.edu.cn).